6-29-2017

Spatial variability of CO < inf> 2 uptake in polygonal tundra: Assessing low-frequency disturbances in eddy covariance flux estimates

Norbert Pirk
Institutionen för Naturgeografi och Ekosystemvetenskap, Lunds Universitet

Jakob Sievers
Aarhus Universitet

Jordan Mertes
Michigan Technological University, jrmertes@mtu.edu

Frans Jan W. Parmentier
UiT The Arctic University of Norway

Mikhail Mastepanov
Institutionen för Naturgeografi och Ekosystemvetenskap, Lunds Universitet

See next page for additional authors

Biogeosciences, 14, 3157–3169, 2017
https://doi.org/10.5194/bg-14-3157-2017

Biogeosciences Open Access EGU

Spatial variability of CO_2 uptake in polygonal tundra: assessing low-frequency disturbances in eddy covariance flux estimates

Norbert Pirk[1,2], **Jakob Sievers**[3], **Jordan Mertes**[2,4], **Frans-Jan W. Parmentier**[5], **Mikhail Mastepanov**[1,3], **and Torben R. Christensen**[1,3]

[1]Department of Physical Geography and Ecosystem Science, Lund University, Sölvegatan 12, 22362 Lund, Sweden
[2]Geology Department, The University Centre in Svalbard, UNIS, 9171 Longyearbyen, Norway
[3]Arctic Research Centre, Aarhus University, Aarhus, Denmark
[4]Department of Geological and Mining Engineering and Sciences, Michigan Technological University, 630 Dow Environmental Sciences, 1400 Townsend Drive, Houghton, MI 49931, USA
[5]Department of Arctic and Marine Biology, UiT – The Arctic University of Norway, Postboks 6050 Langnes, 9037 Tromsø, Norway

Correspondence to: Norbert Pirk (norbert.pirk@nateko.lu.se)

Received: 10 December 2016 – Discussion started: 14 December 2016
Revised: 16 May 2017 – Accepted: 17 May 2017 – Published: 29 June 2017

Abstract. The large spatial variability in Arctic tundra complicates the representative assessment of CO_2 budgets. Accurate measurements of these heterogeneous landscapes are, however, essential to understanding their vulnerability to climate change. We surveyed a polygonal tundra lowland on Svalbard with an unmanned aerial vehicle (UAV) that mapped ice-wedge morphology to complement eddy covariance (EC) flux measurements of CO_2. The analysis of spectral distributions showed that conventional EC methods do not accurately capture the turbulent CO_2 exchange with a spatially heterogeneous surface that typically features small flux magnitudes. Nonlocal (low-frequency) flux contributions were especially pronounced during snowmelt and introduced a large bias of $-46\,gC\,m^{-2}$ to the annual CO_2 budget in conventional methods (the minus sign indicates a higher uptake by the ecosystem). Our improved flux calculations with the ogive optimization method indicated that the site was a strong sink for CO_2 in 2015 ($-82\,gC\,m^{-2}$). Due to differences in light-use efficiency, wetter areas with low-centered polygons sequestered 47 % more CO_2 than drier areas with flat-centered polygons. While Svalbard has experienced a strong increase in mean annual air temperature of more than 2 K in the last few decades, historical aerial photographs from the site indicated stable ice-wedge morphology over the last 7 decades. Apparently, warming has thus far not been sufficient to initiate strong ice-wedge degradation, possibly due to the absence of extreme heat episodes in the maritime climate on Svalbard. However, in Arctic regions where ice-wedge degradation has already initiated the associated drying of landscapes, our results suggest a weakening of the CO_2 sink in polygonal tundra.

1 Introduction

Arctic tundra is often covered with polygonal ground patterns created by subsurface ice wedges (Leffingwell, 1915; Mackay, 1974; Romanovskii, 1985; Minke et al., 2007). While ice wedges need centuries or millennia to form through the infiltration and refreezing of meltwater in thermal contraction cracks, they have been reported to degrade rapidly during the last decades with permafrost warming, which significantly alters soil drainage and moisture (Fortier et al., 2007; Liljedahl et al., 2016). Especially in the high Arctic where permafrost warming occurs the fastest (Romanovsky et al., 2010), these hydrological changes can influence the land–atmosphere exchange of greenhouse gases, such as carbon dioxide (CO_2), which could affect the long-term carbon sink function of these ecosystems (Schuur et al., 2015; Jorgenson et al., 2015).

Carbon dioxide fluxes in polygonal tundra are characterized by large spatial variability, which complicates their ac-

curate assessment over larger areas (McGuire et al., 2012). On a scale of hectares to km^2, the micrometeorological eddy covariance (EC) technique has become widely used to measure the net ecosystem exchange of CO_2 (NEE) because it provides a good compromise between directness of measurement, ecosystem disturbance, and technical reliability. The EC technique estimates NEE integrated over an upwind footprint area based on point measurements of the covariance of vertical wind speed and CO_2 concentration (Aubinet et al., 2012). Careful calculations have been found to provide defensible estimates of the true CO_2 flux, with the main systematic uncertainties stemming from nonsteady atmospheric conditions, heterogeneous surfaces, and complex terrain (Baldocchi, 2003). Large-scale surface heterogeneity has been observed and simulated to induce thermal circulations on the mesoscale that can impede the turbulent flux estimation (Mahrt et al., 1994; Inagaki et al., 2006), and complex terrain may lead to horizontal advection of gases and thereby biased flux estimations (Finnigan et al., 2003; Aubinet et al., 2010). Finnigan et al. (2003) showed that the averaging operation and coordinate rotation commonly applied in EC flux calculations can lead to co-spectral distortions and a loss of flux in measurements over tall canopies (forests), even though it is not evident that the same holds for the short-statured vegetation of the tundra where measurements are taken well above the roughness sublayer. Other difficulties relate to the employed measurement instruments, such as open-path gas analyzers, which can introduce a bias due to surface heating of the instrument itself (Burba et al., 2008). Results from different conventionally used software packages for EC calculations have been shown to agree in temperate grasslands and forests (Fratini and Mauder, 2014), but the typically low flux magnitudes in high Arctic environments pose considerable challenges for the correct estimation of EC fluxes (Sievers et al., 2015a). Special care must be taken during the long cold season when small CO_2 releases can add up to a significant portion of the total annual carbon budget (Fahnestock et al., 1999; Björkman et al., 2010; Lüers et al., 2014).

Across the Arctic tundra, previous studies have shown differing CO_2 budgets depending on the characteristics of the landscape. Eddy covariance CO_2 flux measurements from a well-studied high Arctic tundra site in northeastern Greenland indicate a considerable annual carbon sink ($-64\,gC\,m^{-2}$) in a wet fen (Soegaard and Nordstroem, 1999), while the neighboring dry heath constitutes a weaker sink on average ($-21\,gC\,m^{-2}$) (Lund et al., 2012). Measurements from Alaskan tussock tundra show that nongrowing season releases of CO_2 can also exceed the growing season uptake, rendering the ecosystem a small net annual source ($+14\,gC\,m^{-2}$) (Oechel et al., 2014). A wet tussock grassland in NE Siberia was found to be a moderate annual sink ($-38\,gC\,m^{-2}$) (Corradi et al., 2005), while wet polygonal tundra in the Lena River delta was estimated to be a weaker annual CO_2 sink ($-19\,gC\,m^{-2}$) (Kutzbach et al., 2007). Some of these studies rely on modeled fluxes to fill large data gaps during wintertime, which increases the uncertainty in the annual sums.

As opposed to other permafrost-underlain regions where soils could become wetter in the future (Natali et al., 2011; Johansson et al., 2013), polygonal tundra is predicted to dry upon permafrost degradation (Liljedahl et al., 2016); the ground above melting ice wedges subsides, which interconnects the polygon troughs and creates an effective drainage network for the wet polygon centers (Fortier et al., 2007). This simultaneous wetting of polygon troughs and drying of polygon centers is a signature that can be detected in time series of historical aerial photographs to provide large-scale evidence of the process (Necsoiu et al., 2013). Liljedahl et al. (2016) described such ice-wedge degradation as a widespread Arctic phenomenon that changed surface drainage patterns in less than 1 decade. To study the progressive change in plant communities and biogeochemistry following such a disturbance, space-for-time substitutions have proven to be a powerful tool (Rastetter, 1996). The associated hydrological changes have thus been linked to significant changes in carbon fluxes in Alaskan polygonal tundra during the growing season (Lara et al., 2015; Vaughn et al., 2016), but their year-round effect on an ecosystem's CO_2 budget has yet to be quantified.

Such an assessment could be improved by high-resolution topographical surveys using unmanned aerial vehicles (UAVs). Apart from the visual picture that UAVs provide, series of photographs from multiple angles allow for the reconstruction of the 3-D geometry of the surface (Ullman, 1979; Westoby et al., 2012), which can give valuable insights into the drainage patterns. In the present study, we explore the potential of this technique in combination with EC CO_2 flux measurements in polygonal tundra on Svalbard to characterize the spatial heterogeneity of the ecosystem. We aim to understand how the spatial heterogeneity and larger-scale disturbances affect EC flux estimates by investigating the spectral composition of the EC signal. We further relate the spatial differences in NEE to the observed historical and predicted future evolution of ice-wedge polygons.

2 Materials and methods

2.1 Site description

The field site is located at the bottom of a large, permafrost-underlain, glacial valley called Adventdalen on Spitsbergen, Svalbard, approximately 6 km from a fjord (78°11′ N, 15°55′ E). The surrounding mountains feature plateaus of around 450 m a.s.l. and peaks and ridges of up to 1000 m a.s.l., which are still partly glaciated (De Haas et al., 2015). Wind directions are generally oriented along the valley with dominating easterlies in wintertime (coming from inland Spitsbergen) and an approximately even distribution

of easterlies and westerlies in summertime (westerlies coming from the fjord). Long-term statistics indicate that wind speeds in Adventdalen are below 5 m s^{-1} for about 70 % of the year (and below 10 m s^{-1} for about 97 %) with the most frequent wind speed at about 3 m s^{-1}. The mean annual air temperature at the closest weather station (Svalbard airport, approximately 10 km away) was −6.7 °C between 1961 and 1990 (Førland et al., 2012); it increased to −3.75 °C in the period between 2000 and 2011 (Christiansen et al., 2013). The total annual precipitation is about 190 mm, of which about half falls as snow (Førland et al., 2012). The measurement site is located on a river terrace on the flat part of a large alluvial fan where the ground is patterned by ice-wedge polygons (Christiansen, 2005; Harris et al., 2009). These coarse alluvial deposits are covered with a few tens centimeters of organic material and fine-grained eolian deposits (loess), which typically stem from wind erosion in the braided riverbed when it dries out in autumn (Bryant, 1982; Oliva et al., 2014). The site's soil organic carbon content in the uppermost 100 cm of soil is about 30 kgC m^{-2} (P. Kuhry, personal communication, 2016). The vegetation at the Adventdalen site features *Salix polaris* in drier areas and *Eriophorum scheuchzeri* and *Carex subspathacea* in wetter locations. The moss cover is sparse in drier polygons where shrubs dominate the vegetation community, while the wetter areas at local depressions feature an almost continuous moss cover. Within individual polygons, the moss coverage typically increases from the drier rim to the wetter center.

2.2 Measurement setup

The EC setup consisted of a top-mounted ultrasonic anemometer (USA-1; Metek GmbH, Germany) and an infrared gas analyzer (Li-7200; Li-Cor Inc., USA), both of which sampled and recorded data at a rate of 10 Hz. The measurement height was 2.8 m above ground level. From there the gas was pumped to the Li-7200 at a flow rate of 15 L min^{-1} via a 1 m long insulated intake tube supplied by the manufacturer.

Ancillary meteorological measurements (e.g., solar radiation, snow and soil temperatures) were collected on and around the same tower, sampled every 10 s, and averaged to 30 min values. Due to the relatively remote location without line power, the system was supplied by lead–acid batteries charged by a wind generator (350 W peak output), solar panels (275 W peak output), and a fuel cell in summertime (90 W).

Complementary to the EC setup, we measured NEE in the EC footprint with a set of five transparent, automatically operated flux chambers using the closed-chamber technique. These chambers were connected to a gas analyzer (SBA-4; PP Systems, UK) that measured CO_2 concentrations at a rate of 0.625 Hz. Flux estimates were derived from an exponential least-squares regression of the 5 min closure time of the concentration time series. The details of this measurement system and flux estimation procedure are provided in Pirk et al. (2016b) and the references therein.

To assess differences in the active layer depth, thaw depths were probed at the centers of 30 polygons in the EC footprint at the end of August 2016.

2.3 Data processing

Eddy covariance flux estimates were derived using the recently proposed ogive optimization method (version 1.0.5; toolbox publicly available through the Mathworks file exchange) (Sievers et al., 2015b). In this context, ogives are cumulative co-spectra of vertical wind speed (w) and CO_2 concentration, which is denoted Og (w, CO_2), i.e., a spectral decomposition of the EC flux estimate. The method optimizes a spectral distribution model (Desjardins et al., 1989; Lee et al., 2006; Foken et al., 2006) to a density map of 14 000 ogives obtained by varying the dataset length and detrending interval. The key to this method is the assumption of a dynamic spectral gap between often overlapping spectral flux contributions (Sievers et al., 2015b). This approach effectively separates the turbulent flux from contributions of larger-scale motions (mesoscale atmospheric movements), which can give nonlocal flux contributions at low frequencies (Aubinet et al., 2012; Sievers et al., 2015b).

To further investigate the effect of low-frequency contributions, we compared ogive optimization to the widely used EddyPro software package (Li-Cor Inc.; version 6.1.0), following the conventional assumption about the presence of a fixed spectral gap corresponding to the 30 min flux averaging interval. We used simple linear de-trending and applied spectral corrections according to Moncrieff et al. (1997, 2004) (EddyPro default).

Both EddyPro and ogive optimization perform basic quality control and preprocessing of the 10 Hz raw data following Vickers and Mahrt (1997) (e.g., gap detection, spike removal, signal alignment, anemometer tilt correction). Unacceptable raw data were not processed further. To ensure sufficient turbulent mixing near the surface, we also filtered out data points with a friction velocity smaller than 0.1 m s^{-1} for both methods. Ogive optimization furthermore only accepts periods with a negative momentum flux (i.e., directed toward the ground surface) in the mid-frequency range (tested at around 0.032 Hz), which is the energy-containing range. Following Foken and Wichura (1996), EddyPro fluxes were additionally filtered for nonsteady wind conditions (discarding fluxes with quality flag 2). Calculated ogive optimization fluxes, on the other hand, were only discarded if the modeled ogive spectral distribution could not describe the data sufficiently. These filters, in addition to downtime caused by technical problems, led to an overall data coverage with valid fluxes of 45 % in 2015 for the ogive optimization and 35 % for EddyPro. A large number of these flux calculations have been visually inspected to ensure that the methods performed as expected. In this analysis, we noticed that the automati-

cally determined time lags between w and CO_2 concentration varied unrealistically, which introduced noise to the fluxes, especially at low magnitudes. We therefore used a constant value of 0.3 s (i.e., the typically expected time lag given our setup) for the flux calculation with both methods.

We mainly focused on data collected between September 2014 and December 2015 when data quality and coverage were the highest. Carbon dioxide concentrations collected in 2013 were only recorded as molar densities without the cell pressure necessary for a sample-by-sample conversion to mixing ratios according to the Webb–Pearman–Leuning correction proposed by Sahlée et al. (2008), which is currently the only option implemented in the ogive optimization software. Hence, we only report 2013 fluxes from EddyPro as supplementary support for our findings.

Subsequently, the calculated NEE was used to determine the ecosystem's light response characteristics during the snow-free period (the beginning of June until the end of September). One way to parameterize the relationship between NEE and incoming photosynthetically active radiation (PAR) is the Misterlich function:

$$\mathrm{NEE} = -\left(F_{\mathrm{csat}} + R_{\mathrm{d}}\right)\left(1 - \exp\left(-\frac{\alpha\,\mathrm{PAR}}{F_{\mathrm{csat}} + R_{\mathrm{d}}}\right)\right) + R_{\mathrm{d}}, \quad (1)$$

where the three parameters F_{csat}, R_{d}, and α correspond to the flux at light saturation, dark respiration, and light-use efficiency, respectively (e.g., Falge et al., 2001). Such light response curves can yield further insights into the underlying drivers of NEE. These parameters were derived from least-squares regressions of measured NEE and PAR (derived from shortwave incoming radiation) in a rolling time window of 10 days, which was successively increased by 1 day if fewer than 100 valid NEE-PAR measurements were available, following Lund et al. (2012).

For cumulative flux calculations and annual sums we employed the gap-filling algorithm proposed by Reichstein et al. (2005), which operates on the basis of mean diurnal variations in temperature, incoming shortwave radiation, and vapor pressure deficit as drivers for NEE. As some of the gaps in our NEE measurements were caused by power outages (when the entire measurement system shut down), the ancillary data for gap filling were taken from the New Adventdalen Weather Station (run by the University Centre in Svalbard) with a distance of about 2.5 km from our site. This procedure yielded the best gap-filling quality (class A) in 96 % of the flux estimates that had to be gap filled in 2015. Still, gaps in NEE measurements can be assumed to dominate the total random error in the annual sums (Aurela et al., 2002). To quantify this uncertainty, we tested the sensitivity of the annual sums to artificially added gaps in the NEE time series. Since the uncertainty introduced by a gap depends on its length and the time of year, we repeated the gap filling on 300 different time series obtained by adding single gaps of between 1 and 23 days (i.e., 2 days longer than our longest gap) that were equally distributed over the year (starting every 15 days). The resulting distribution of annual sums was used to assess the result's random error.

The EC footprint estimation was performed according to Kljun et al. (2015) using a fixed zero-plane displacement of 10 cm and a roughness length of 1 cm. Wind and turbulence parameters were derived from 30 min intervals, while the additionally needed boundary layer height was taken from the closest point of the ERA-Interim meteorological reanalysis (Dee et al., 2011).

2.4 Topographical survey

We conducted a topographical survey of the Adventdalen ice-wedge site by employing photogrammetry with aerial photographs to produce a visual map and digital elevation model. To this end, 135 photographs were taken with a camera (GoPro Hero3+ Black Edition) from a UAV (DJI Flame Wheel F550) at a height of 60 m a.g.l. in June 2015. This survey covered an area of about 0.1 km^2 at a ground resolution of about 3.2 cm $pixel^{-1}$; 22 ground control points were collected with a differential GPS (Leica GPS1200 SmartRover) to ortho-rectify the images and estimate the uncertainty in the resulting elevation model (see Fig. S5 in the Supplement for details). The GPS data were post-processed and differentially corrected using data from the local Longyearbyen GNSS satellite base station (LYRS), which are freely available from the Norwegian Mapping Authority. The photogrammetric processing was performed using Agisoft PhotoScan (Agisoft LLC, St. Petersburg, Russia), which implements the structure-from-motion technique to reconstruct the 3-D geometry of the ground surface from a sequence of photographs taken from multiple viewpoints (Ullman, 1979; Snavely et al., 2008; Westoby et al., 2012; Lucieer et al., 2014).

To assess the evolution of the morphology of the ice-wedge site, we compared our map from 2015 to historical aerial photographs taken in 1948, 1961, and 1990, which were georeferenced with the 2015 map as a reference. Reliably quantifying the changes between these images was complicated by different shadows and differences in the overall soil moisture when the images were taken, so we only performed a qualitative change detection by visual comparison.

3 Results

Figure 1 shows the results of the topographical survey and the EC footprint for June 2015. As the wind direction typically aligns with the valley's direction, there are two clearly distinct footprint areas in the NW and ESE. The high resolution of this elevation map resolves small elevation differences of only a few decimeters, which can be seen to affect surface inundation and soil wetness. Both footprints have overall surface slopes toward the edge of the river terrace in the north (approximately 0.75 % slope), but their drainage pat-

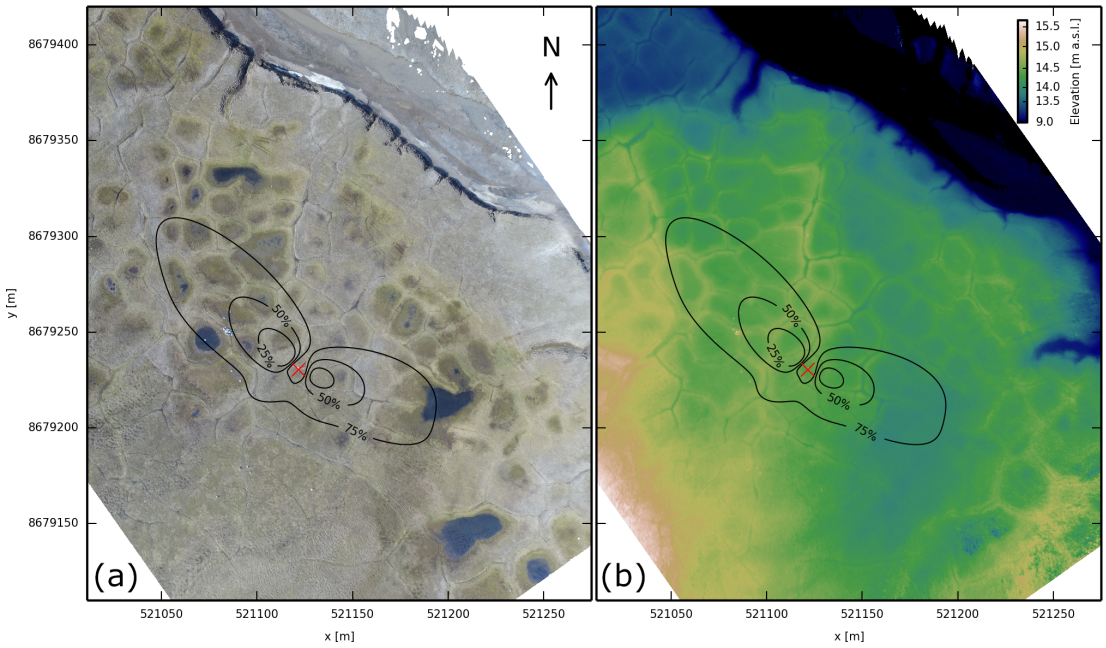

Figure 1. Map of the site in Adventdalen (coordinates in UTM zone 33X). The red cross marks the EC tower, around which the contour lines indicate the area's relative contribution to the EC signal (footprints) averaged over June 2015. Six automatic flux chambers are located in the NW footprint (bright dots). **(a)** Ortho-rectified aerial photograph from the end of June 2015. **(b)** Corresponding surface elevation with an estimated vertical uncertainty of 0.2 m.

terns appear to be separated, creating a wetter sub-catchment in the NW than in the ESE. Low-centered polygons dominate the site, but the NW features more distinctly wet polygon centers. The thaw depth at the centers of the polygons around the EC tower was 66 cm ± 9 cm (mean ± SD; sample size $N = 30$) by the end of August. Based on the polygons in the 50 % EC footprint, the drier ESE fetch area featured a thaw depth of 69 cm ± 8 cm ($N = 4$) while the wetter NW featured 79 cm ± 4 cm ($N = 4$); this is not a statistically significant difference ($p = 0.10$).

The shown surface heterogeneity is likely to lead to spatial variations in NEE in the EC footprint. To assess this effect and mesoscale disturbances, we investigated the spectral composition of the EC signal by looking at the ogives of vertical wind speed and CO_2 concentration. Particularly around the time of snowmelt, we often found a mismatch between lower and higher frequencies, indicating different local and nonlocal flux contributions. Figure 2 shows an example from this period comparing the ogives of conventional flux calculations produced by EddyPro and ogive optimization flux estimation based on the ogive density map. While all frequencies fully contribute to the conventional flux estimation, frequencies can obtain less weight with the ogive optimization method if they cannot be described by the ogive spectral distribution model. In the given example, this conceptual difference in the methods means that ogive optimization indicated a CO_2 release, while EddyPro indicated uptake. Spectral corrections had a comparably small effect. The ogive optimization model indicates that all relevant flux contributions are carried by turbulence with a scale shorter than about 25 s in this example (which does not, however, mean that 25 s is sufficient to determine a 30 min flux). During this period in May and June, the surface was a mix of patches of snow-free soil, remaining snow, and meltwater ponds (when a net CO_2 uptake can be considered unlikely; see Fig. 2b). The low-frequency contributions also depend on larger-scale atmospheric movements, while the local turbulent flux is represented better in the mid- to high-frequency range. Such frequency mismatches (high-frequency CO_2 release, but low-frequency uptake) were frequently observed in our data and their effect was relatively the largest for the small nongrowing season fluxes (see Fig. S1 for additional ogive examples and Fig. S3a for a flux comparison). The shifts between the release and uptake of CO_2 typically occurred at frequencies below 10^{-1} Hz, corresponding to recorded eddies with a diameter of typically more than 30 m at the given wind speed. During the growing season, fluxes from both methods typically agreed. Photos of the site in different seasons are given in Fig. S6.

Since the frequency mismatches cannot be resolved in conventional calculations, we focus on the NEE fluxes calculated by the ogive optimization method for the ecosystem characterization. Figure 3 shows the gap-filled NEE fluxes of 2015 as fingerprint plots and cumulative sums, which were also calculated after separately gap filling the measurements of the two distinct footprints (NW and ESE). These results

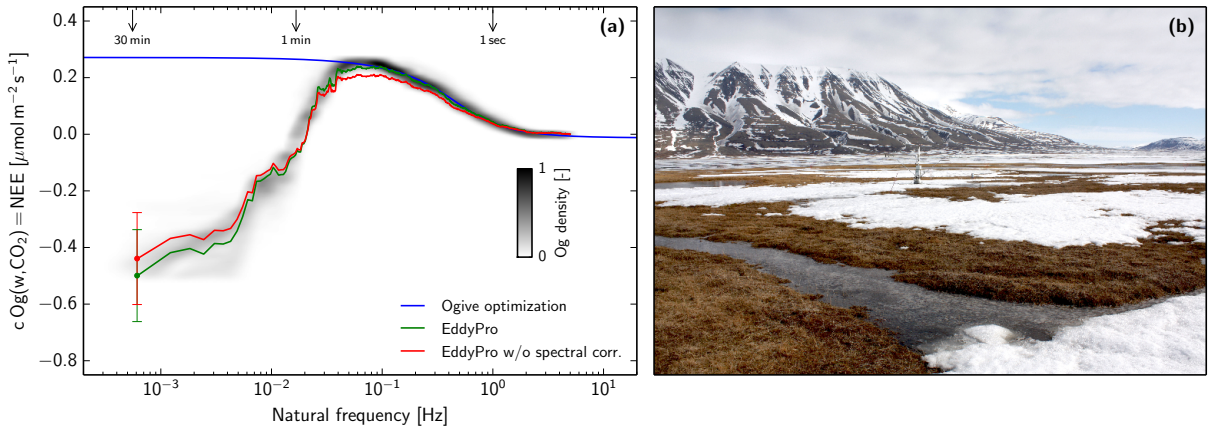

Figure 2. Example of the CO_2 flux estimation during snowmelt. **(a)** Ogive on 31 May 2015 at 15:00 LT showing a mismatch between low and high frequencies. While ogive optimization estimates a net CO_2 release, EddyPro (with and without spectral corrections after Moncrieff et al., 1997, 2004) indicates an uptake. Average horizontal wind speed 5.2 m s^{-1} from NW (313°), air temperature 4.5 °C, quality flag 0. The arrows on the top indicate the corresponding timescales. **(b)** Photo of the environment around the flux tower on 27 May 2015 at 12:00 LT during snowmelt.

indicate that the growing season in 2015 started on 14 June and ended 28 August (defined as the first until the last day of net CO_2 uptake). The results from EddyPro indicated the same date for the end of the growing season, while its start was already suggested 1 month before snowmelt. The fingerprint plot (Fig. 3a) shows that there can even be CO_2 uptake at midnight during the polar day in the summer. While the drier ESE yielded an annual carbon balance of -62 gC m^{-2}, the wetter NW yielded -91 gC m^{-2}. The annual balance of the combined footprint (using all fluxes without separating periods of different wind directions) was -82 gC m^{-2} in 2015. The corresponding value based on the EddyPro flux calculations was -128 gC m^{-2}, which we consider biased by the abovementioned low-frequency contributions. The relatively narrow probability distributions of the annual sums (based on gap-filling uncertainties) demonstrate the significance of the differences between the NW and ESE footprints and between the ogive optimization and EddyPro methods. Relatively large annual sinks are supported by our automatic closed-chamber measurements in the NW footprint, which show good agreement and correlation ($0.75 < r < 0.88$; $p < 0.0001$) with the EC fluxes (see Fig. S3b). In 2013, the EddyPro calculations yielded a smaller total annual CO_2 balance of -79 gC m^{-2} (see Fig. S2d), whereas ogive optimization fluxes could not be calculated from 2013 raw CO_2 measurements (see Sect. 2.3).

Many of the spatial differences in the annual CO_2 budget stem from the growing season when NEE is strongly affected by PAR. Figure 4 shows examples of the derived light response curves and the evolution of the associated dark respiration and light-use efficiency throughout the growing season. Both dark respiration and light-use efficiency were typically higher in the wetter footprint (NW) than in the drier (ESE), which is consistent with the larger annual uptake in the NW than the ESE. At the beginning and end of the growing season, the determination of the flux at light saturation (F_{csat}) was associated with relatively large uncertainties because NEE and PAR varied relatively little. During the peak growing season, F_{csat} was about 6.6 μmol m^{-2} s^{-1} for both footprints. The sum of F_{csat} and R_d can be used to estimate the gross primary productivity at light saturation, which was found to be -11.0 μmol m^{-2} s^{-1} in the NW and -8.3 μmol m^{-2} s^{-1} in the ESE. During snow-covered conditions outside the growing season, our measurements indicated an overall decreasing trend in the small CO_2 releases throughout winter, which was modulated by increases during strong winds (see Fig. S4). Soil temperature, on the other hand, had no strong effect on the wintertime CO_2 release despite a large variation of more than 25 K (see Fig. S4c).

Figure 5 shows a time series of ortho-rectified aerial photographs covering the same area as Fig. 1. Despite the differences in image quality, shadows, and overall soil moisture on the days the images were taken, the time series still gives an impression of the development of the polygon morphology. All images show the same low-centered polygons with centers that are about equally inundated (except in 1990 when the area was drier in general). There was no clear lateral expansion or degradation of the polygon troughs. Neither the ponds nor the troughs became more interconnected or wet in general, so there are no clear signs of differential ground subsidence at this site. Other areas with ice-wedge polygons in Adventdalen also indicated the same stable morphology during the last 7 decades (see Fig. S7). Between 1990 and 2015, some erosion on the edge of the river terrace occurred. The exact speed of this edge erosion is hard to quantify due to the shadows in this area, but it did not exceed 3 m over these 15 years.

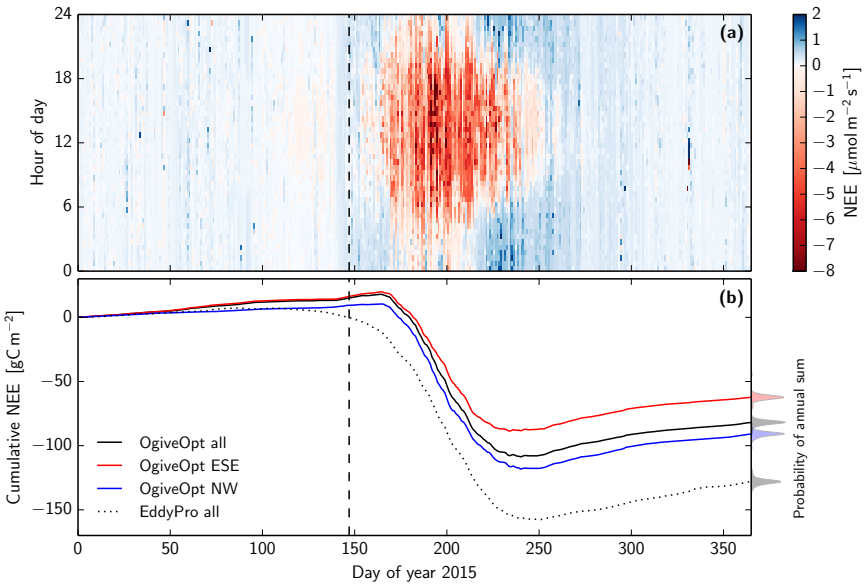

Figure 3. Gap-filled NEE fluxes for 2015. **(a)** Fingerprint plot of ogive optimization results. **(b)** Corresponding cumulative sums based on all valid measurements (black) and separately gap filled for the two footprints (colored). The probability distributions shown on the right indicate the estimated uncertainty in the annual sum due to data gaps and gap filling. The dashed line marks the time during snowmelt when daily average albedo dropped below 0.3 (27 May 2015).

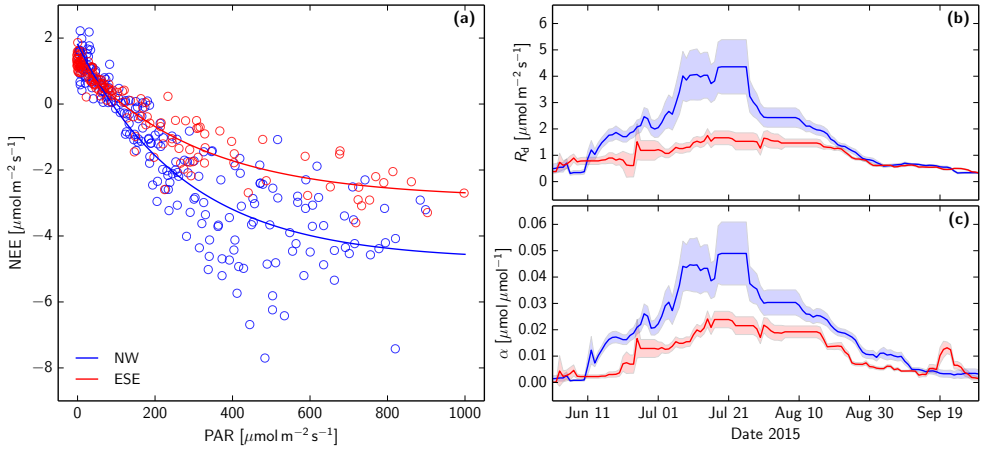

Figure 4. Growing season NEE light response curves based on the ogive optimization method. **(a)** Examples from the time window around 18 August 2015 from the two distinct footprints. **(b)** Time series of dark respiration parameters. **(c)** Corresponding graph for light-use efficiency. The shaded bands indicate the statistical standard error in the parameters.

The photograph from 1990 was taken in the near-infrared range and is shown in false colors. Vegetation, bare soil, and open water reflect near-infrared light differently, so this image clearly depicts these surfaces. The strong red tones in the NW footprint correspond to the relatively high vegetation density in this area, which is also seen in Fig. 1. The river in the NE appears in a blue tone, while the darker spots in the SW corner of the image correspond to an area with bare soil brought to the surface by cryoturbation.

4 Discussion

Our measurements demonstrate the high sensitivity of carbon cycling to small topographic differences in permafrost-underlain Arctic tundra. Ice-rich permafrost is particularly vulnerable to warming, with large increases in permafrost degradation documented in the last 2 decades (Jorgenson et al., 2006; Osterkamp et al., 2009; Grosse et al., 2011). Liljedahl et al. (2016) observed pan-Arctic permafrost degradation in polygonal tundra, which dramatically changed the local drainage patterns and water balance on sub-decadal

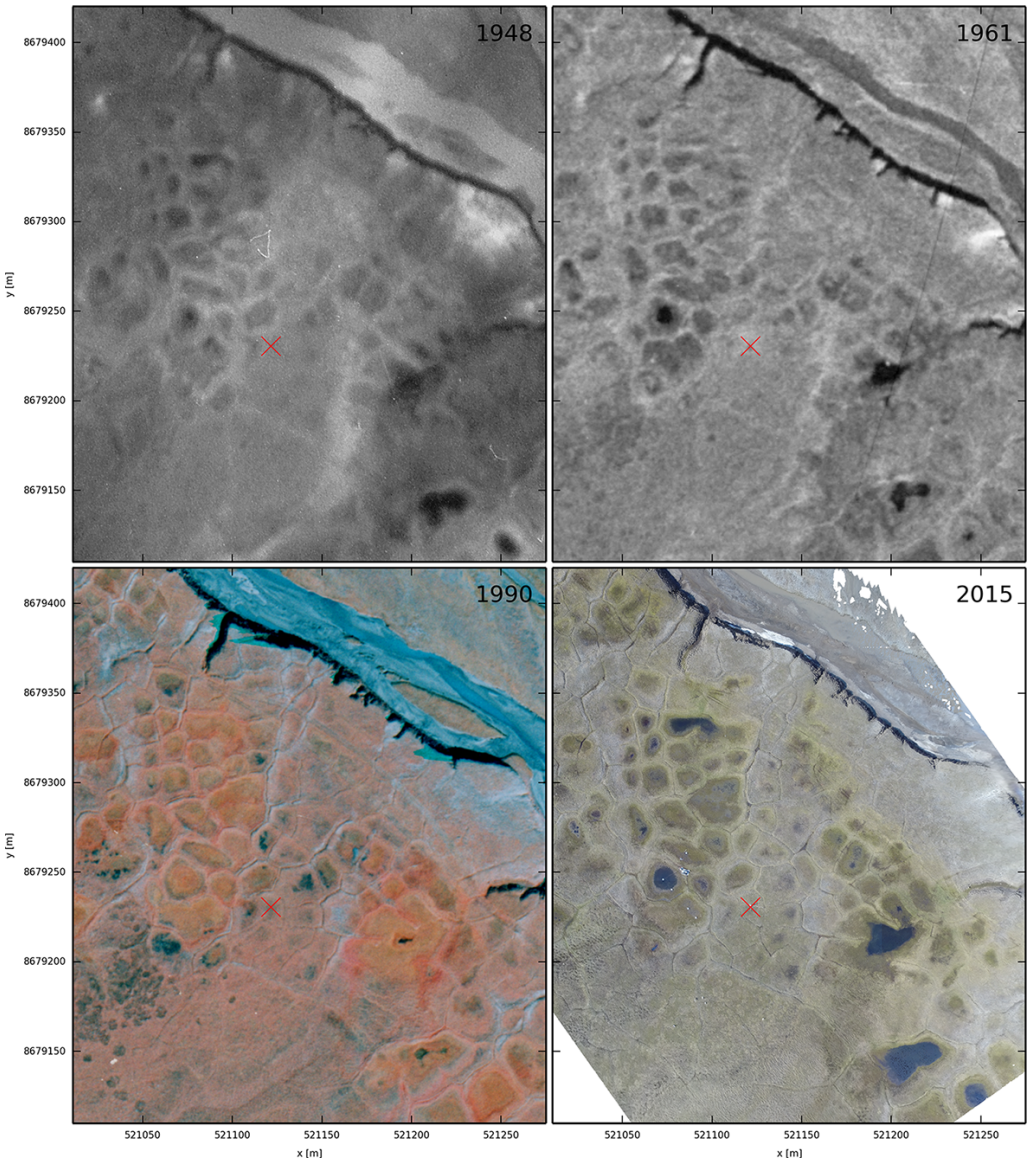

Figure 5. Time series of images of the Adventdalen site showing little sign of differential ground subsidence, which would indicate ice-wedge degradation. The image from 2015 is the same as shown in Fig. 1, while historical photographs were provided by the Norwegian Polar Institute (reference numbers S48-5181, S61-3301, and S90-5273). The images from 1948 and 1961 were taken on panchromatic film, and the image from 1990 is a near-infrared (false color) photograph. The red cross marks the EC tower.

timescales. Ice-wedge melting and the associated differential ground subsidence is expected to interconnect formerly separated trough networks and thereby increase the drainage of polygon centers (Necsoiu et al., 2013; Jorgenson et al., 2015; Liljedahl et al., 2016). At a later stage this process transforms low-centered polygons into high-centered polygons and leads to the overall drying of the entire landscape. In such cases, the space-for-time substitution of our two distinct footprint areas in Adventdalen would suggest a corresponding lessening of CO_2 sinks in degrading polygonal tundra.

However, our comparison of aerial photographs taken between 1948 and 2015 shows that there is no dramatic ice-wedge degradation at our site on Svalbard. Nearby areas with polygonal tundra in Adventdalen have also been stable during the last 7 decades, despite the measured increase of 2.95 °C in mean annual air temperatures between the periods 1961–1990 and 2000–2011 (Førland et al., 2012; Christiansen et al., 2013; Nordli et al., 2014). The maritime climate on Svalbard prevents episodes with extremely high summer temperatures, which have been hypothesized to trigger ice-wedge degradation (Jorgenson et al., 2006; Liljedahl et al., 2016). It appears that gradual climate warming alone

has so far not been sufficient to initiate strong ice-wedge degradation in Adventdalen. Another reason for the apparent stability of the ice wedges at our site could be the relatively small surface slope of typically less than 1 %, which hinders the development of an effective drainage system of degraded troughs. Generally speaking, ice-wedge stabilization can also be caused by negative feedbacks, such as increased plant growth in degraded troughs, which cools the soil above the ice wedge (Jorgenson et al., 2015). Despite these mechanisms and observations, the strong temperature increase on Svalbard may eventually lead to the gradual degradation of ice wedges in Adventdalen, which we argue will lessen the CO_2 sink of this ecosystem.

The overall annual CO_2 balance of $-82\,\mathrm{gC\,m^{-2}}$ seems surprisingly large given the high northern location of the site with its typically shallow organic horizon in the soil (5–10 cm). The good agreement of EC and automatic closed-chamber measurements, however, confirms the relatively high uptake fluxes in the snow-free period (see Fig. S3b). The comparison of the light response curve parameters to other Arctic sites also indicates high but realistic growing season productivity. Mbufong et al. (2014) derived these parameters from 12 Arctic tundra sites during the peak growing season and report R_d between 0.6 and $3.9\,\mu\mathrm{mol\,m^{-2}\,s^{-1}}$ and α between 0.011 and $0.057\,\mu\mathrm{mol\,\mu mol^{-1}}$. Peak season parameters for the drier footprint (ESE; $R_\mathrm{d} \sim 1.7\,\mu\mathrm{mol\,m^{-2}\,s^{-1}}$, $\alpha \sim 0.024\,\mu\mathrm{mol\,\mu mol^{-1}}$) at the Adventdalen site lie well in the center of this range, while the wetter footprint (NW; $R_\mathrm{d} \sim 4.3\,\mu\mathrm{mol\,m^{-2}\,s^{-1}}$, $\alpha \sim 0.049\,\mu\mathrm{mol\,\mu mol^{-1}}$) lies on the upper end of this reported range. These values, in combination with the relatively large amount of incoming shortwave radiation at 78° N during summertime, explain the large carbon sink in Adventdalen. The summertime CO_2 sink in Adventdalen is comparable to this season's CO_2 balance in a coastal wet sedge tundra ecosystem in Barrow, Alaska (-105 to $-162\,\mathrm{gC\,m^{-2}}$) (Harazono et al., 2003). The wetter areas, in particular, lose some carbon through methane emissions, but automatic chamber measurements at Adventdalen indicate that these losses are not expected to exceed $6\,\mathrm{gC\,m^{-2}}$ per year (Pirk et al., 2016a). We consider the export of dissolved organic carbon negligible because the small surface slope and limited conductivity prevents a pronounced lateral water runoff.

The grazing pressure from Svalbard reindeer could represent another type of carbon loss that has not been quantified in the present study. Moreover, Wegener and Odasz-Albrigtsen (1998) observed that plants in Adventdalen balance the consumption by reindeer with increased plant productivity. While such interactions influence the carbon budget of the ecosystem, they do not affect the discrepancy we found between the two EC flux calculation methods.

The drivers of cold season emissions of CO_2 from high Arctic tundra are still understudied because technical challenges and low flux magnitudes often complicate continuous in situ flux measurements. Our wintertime flux measurements from Adventdalen were found to decrease slightly throughout winter. Episodic flux increases correlated with wind speed, suggesting a convective mixing of the snowpack gas reservoir as observed in other studies from lower latitudes (Takagi et al., 2005; Seok et al., 2009; Smagin and Shnyrev, 2015). The missing relation between soil temperature and measured wintertime CO_2 release could suggest a decoupling of CO_2 production and release caused by the physical blockage of gas diffusion in the soil (Elberling and Brandt, 2003) or through potential ice layers in the snowpack (Pirk et al., 2016a). While the majority of wintertime fluxes were positive, some small uptake fluxes have also been observed during the dark snow-covered period. Unlike reports from other sites (Lüers et al., 2014), these fluxes have no significant impact on the annual CO_2 budget at our site. As photosynthesis by plants or snow algae can be excluded during the dark polar night, one might speculate that the apparent uptakes are caused by abiotic mechanisms, such as the convective mixing of CO_2-depleted gas stored in the snowpack or thermophysical processes related to CO_2 solubility in unfrozen pore water. Yet we found no relationship between uptake situations and changes in snow, air and soil temperatures, or ambient atmospheric CO_2 concentrations that could support potential abiotic mechanisms of CO_2 uptake. The magnitude of these fluxes was also so low compared to biotic flux contributions that they cannot markedly change the overall annual CO_2 balance of the ecosystem and are therefore regarded as noise in this study.

The conceptual definition of turbulent fluxes fundamentally differs in the ogive optimization compared to conventional methods as implemented with EddyPro. While the ogive optimization method assumes a unidirectional flux, which is sometimes better captured in the mid- and high-frequency range, EddyPro includes all frequencies regardless of their direction. The ogive optimization method appeared better suited for the Adventdalen site than conventional processing schemes. Specifically around the snowmelt period, the ogive optimization estimates appear to capture the local flux signal more realistically than conventional calculations, which indicated an onset of the growing season before snowmelt. This contradiction was caused by many bidirectional fluxes, i.e., situations with a consistent CO_2 release reflected in high frequencies and CO_2 uptake reflected in the low-frequency range of the spectrum (see Figs. 2 and S1). The shift between these contributions occurred at frequencies corresponding to eddies with a diameter of more than 30 m, i.e., exceeding the typical dimensions of surface heterogeneity in the footprint area of our site. However, we cannot fully exclude the possibility that the frequency mismatches are caused by flux heterogeneity within the local footprint. It could be possible that the drier areas near the EC tower (reflected better in the high frequencies) are net CO_2 sources, while wetter areas at greater distances from the tower (reflected in the low frequencies) are net CO_2 sinks. A heterogeneous vegetation composition might cause such

flux heterogeneity during snowmelt because, unlike shrubs and sedges, mosses have photosynthetically active tissue that may overwinter so that they can start photosynthesizing at low rates during snowmelt (Oechel, 1976; Tieszen et al., 1980). While some degree of flux heterogeneity is certainly present at any time of year, its effect might be too small to explain the large frequency mismatches observed, particularly during snowmelt. Nevertheless, our observations might incentivize future studies to investigate the frequency dependency of EC footprints. Snowmelt also entails a change in the typical surface roughness length, which is slightly smaller for snow than open tundra vegetation. However, such shifts would be no problem for the functionality of the flux calculation schemes and cannot readily explain bidirectional fluxes, even if the surface roughness is spatially heterogeneous. One might speculate that the systematic occurrences of bidirectional flux are due to an atmospheric layering in which low- and high-frequency eddies circle through air masses with different atmospheric stability and CO_2 concentrations. While the (smaller) high-frequency eddies only reflect one air mass, the (larger) low-frequency eddies reflect two air masses with different CO_2 concentrations. In the specific environment in Adventdalen, such a layering might be induced by the intrusion of CO_2-depleted air at the surface originating from the surrounding mountains by way of katabatic winds or sea breeze circulations from the nearby fjord (Esau and Repina, 2012). However, similar low-frequency shifts were also observed in temperate regions (Finnigan et al., 2003) and in environments with neither pronounced surface heterogeneity nor nearby water bodies, snow, or mountains (Sievers et al., 2015b). Across the different sites we see a tendency for low-frequency shifts to occur predominantly during conditions with small flux magnitudes when the normally dominating mid- and high-frequency contributions can be much smaller than (nonlocal) low-frequency contributions. So perhaps the hypothetical layering of the atmosphere is caused by the repeatedly changing CO_2 flux at the surface in response to diurnal factors, such as changes in incoming solar radiation, which give rise to CO_2 concentration waves propagating vertically into the atmosphere. While such hypotheses remain to be investigated in future studies, we show that these (nonlocal) low-frequency contributions lead to a difference in the annual CO_2 budget of $-46\,\mathrm{gC\,m^{-2}}$ over the course of 1 year (see Fig. 3b). The ogive optimization method is more applicable to these highly heterogeneous Arctic environments dominated by small fluxes because it can separate local and nonlocal flux contributions.

5 Conclusions

The Adventdalen ice-wedge site was a surprisingly strong CO_2 sink in 2015 ($-82\,\mathrm{gC\,m^{-2}}$). Differences in vegetation density and composition led to a significantly higher light-use efficiency in areas with low-centered ice-wedge polygons compared to flat-centered polygons. While dark respiration in the wetter area was also higher than in the drier area, these releases did not compensate for the higher light-use efficiency in the annual CO_2 balance. In 2015, the drier area sequestered 32 % less CO_2 than the wetter area (-62 compared to $-91\,\mathrm{gC\,m^{-2}}$). These results suggest a high sensitivity of CO_2 dynamics to small topographic differences in Arctic tundra ecosystems. With climate warming, ice wedges are predicted to melt and dry out the landscape. Despite strong increases in mean annual air temperatures of more than 2 °C on Svalbard in the last few decades, we see no evidence of ice-wedge degradation compared to historical aerial images. However, further warming may eventually initiate ice-wedge degradation, and our spatial analysis implies a corresponding reduction in the CO_2 sink upon drying. In Arctic polygonal tundra where drying is already occurring, our results therefore suggest a similar weakening of the CO_2 sink function.

Data availability. Maps, measurement data, and processing scripts are available from the authors upon request (norbert.pirk@nateko.lu.se).

The Supplement related to this article is available online at https://doi.org/10.5194/bg-14-3157-2017-supplement.

Competing interests. The authors declare that they have no conflict of interest.

Acknowledgements. The research leading to these results received funding from the European Commission Seventh Framework Programme (FP7) under Grants 238366, 262693, and 282700 and the Nordic Centers of Excellence DEFROST and eSTICC (eScience Tool for Investigating Climate Change at High Northern Latitudes) funded by Nordforsk (grant 57001). We thank Sarah Strand and Andreas Alexander (UNIS) for their work at the Adventdalen site and Sebastian Westermann (University of Oslo) for providing the computational resources needed for the data processing.

Edited by: Fortunat Joos
Reviewed by: Werner Eugster and Lars Kutzbach

References

Aubinet, M., Feigenwinter, C., Heinesch, B., Bernhofer, C., Canepa, E., Lindroth, A., Montagnani, L., Rebmann, C., Sedlak, P., and Van Gorsel, E.: Direct advection measurements do not help to solve the night-time CO_2 closure problem: evidence from three different forests, Agr. Forest Meteorol., 150, 655–664, 2010.

Aubinet, M., Vesala, T., and Papale, D.: Eddy covariance: a practical guide to measurement and data analysis, Springer Science & Business Media, 2012.

Aurela, M., Laurila, T., and Tuovinen, J.-P.: Annual CO_2 balance of a subarctic fen in northern Europe: importance of the wintertime efflux, J. Geophys. Res.-Atmos., 107, ACH 17-1–ACH 17-1, https://doi.org/10.1029/2002JD002055, 2002.

Baldocchi, D. D.: Assessing the eddy covariance technique for evaluating carbon dioxide exchange rates of ecosystems: past, present and future, Glob. Change Biol., 9, 479–492, 2003.

Björkman, M. P., Morgner, E., Cooper, E. J., Elberling, B., Klemedtsson, L., and Björk, R. G.: Winter carbon dioxide effluxes from Arctic ecosystems: an overview and comparison of methodologies, Global Biogeochem. Cy., 24, GB3010, https://doi.org/10.1029/2009GB003667, 2010.

Bryant, I. D.: Loess deposits in lower Adventdalen, Spitsbergen, Polar Res., 1982, 93–103, 1982.

Burba, G. G., Mcdermitt, D. K., Grelle, A., Anderson, D. J., and Xu, L.: Addressing the influence of instrument surface heat exchange on the measurements of CO_2 flux from open-path gas analyzers, Glob. Change Biol., 14, 1854–1876, 2008.

Christiansen, H. H.: Thermal regime of ice-wedge cracking in Adventdalen, Svalbard, Permafrost Periglac., 16, 87–98, 2005.

Christiansen, H. H., Humlum, O., and Eckerstorfer, M.: Central Svalbard 2000–2011 meteorological dynamics and periglacial landscape response, Arct. Antarct. Alp. Res., 45, 6–18, 2013.

Corradi, C., Kolle, O., Walter, K., Zimov, S. A., and Schulze, E.-D.: Carbon dioxide and methane exchange of a north-east Siberian tussock tundra, Glob. Change Biol., 11, 1910–1925, 2005.

De Haas, T., Kleinhans, M. G., Carbonneau, P. E., Rubensdotter, L., and Hauber, E.: Surface morphology of fans in the high-Arctic periglacial environment of Svalbard: Controls and processes, Earth-Sci. Rev., 146, 163–182, 2015.

Dee, D. P., Uppala, S. M., Simmons, A. J., Berrisford, P., Poli, P., Kobayashi, S., Andrae, U., Balmaseda, M. A., Balsamo, G., Bauer, P., Bechtold, P., Beljaars, A. C. M., van de Berg, L., Bidlot, J., Bormann, N., Delsol, C., Dragani, R., Fuentes, M., Geer, A. J., Haimberger, L., Healy, S. B., Hersbach, H., Hólm, E. V., Isaksen, L., Kållberg, P., Köhler, M., Matricardi, M., McNally, A. P., Monge-Sanz, B. M., Morcrette, J.-J., Park, B.-K., Peubey, C., de Rosnay, P., Tavolato, C., Thépaut, J.-N., and Vitart, F.: The ERA-Interim reanalysis: Configuration and performance of the data assimilation system, Q. J. Roy. Meteor. Soc., 137, 553–597, 2011.

Desjardins, R. L., MacPherson, J. I., Schuepp, P. H., and Karanja, F.: An evaluation of aircraft flux measurements of CO_2, water vapor and sensible heat, in: Boundary Layer Studies and Applications, Springer, 55–69, 1989.

Elberling, B. and Brandt, K. K.: Uncoupling of microbial CO_2 production and release in frozen soil and its implications for field studies of arctic C cycling, Soil Biol. Biochem., 35, 263–272, 2003.

Esau, I. and Repina, I.: Wind climate in Kongsfjorden, Svalbard, and attribution of leading wind driving mechanisms through turbulence-resolving simulations, Adv. Meteorol., 2012, 568454, https://doi.org/10.1155/2012/568454, 2012.

Fahnestock, J. T., Jones, M. H., and Welker, J. M.: Wintertime CO_2 efflux from arctic soils: implications for annual carbon budgets, Global Biogeochem. Cy., 13, 775–779, 1999.

Falge E., Baldocchi, D., Olson, R., Anthoni, P., Aubinet, M., Bernhofer, C., Burba, G., Ceulemans, R., Clement, R., Dolman, H., Granier, A., Gross, P., Grünwald, T., Hollinger, D., Jensen, N.-O., Katul, G., Keronen, P., Kowalski, A., Lai, C. T., Law, B. E., Meyers, T., Moncrieff, J., Moors, E., Munger, J. W., Pilegaard, K., Rannik, Ü., Rebmann, C., Suyker, A., Tenhunen, J., Tu, K., Verma, S., Vesala, T., Wilson, K., and Wofsy, S.: Gap filling strategies for defensible annual sums of net ecosystem exchange, Agr. Forest Meteorol., 107, 43–69, 2001.

Finnigan, J. J., Clement, R., Malhi, Y., Leuning, R., and Cleugh, H. A.: A re-evaluation of long-term flux measurement techniques part I: averaging and coordinate rotation, Bound.-Lay. Meteorol., 107, 1–48, 2003.

Foken, T. and Wichura, B.: Tools for quality assessment of surface-based flux measurements, Agr. Forest Meteorol., 78, 83–105, 1996.

Foken, T., Wimmer, F., Mauder, M., Thomas, C., and Liebethal, C.: Some aspects of the energy balance closure problem, Atmos. Chem. Phys., 6, 4395–4402, https://doi.org/10.5194/acp-6-4395-2006, 2006.

Førland, E. J., Benestad, R., Hanssen-Bauer, I., Haugen, J. E., and Skaugen, T. E.: Temperature and precipitation development at Svalbard 1900–2100, Adv. Meteorol., 2011, 893790, https://doi.org/10.1155/2011/893790, 2012.

Fortier, D., Allard, M., and Shur, Y.: Observation of rapid drainage system development by thermal erosion of ice wedges on Bylot Island, Canadian Arctic Archipelago, Permafrost Periglac., 18, 229–243, 2007.

Fratini, G. and Mauder, M.: Towards a consistent eddy-covariance processing: an intercomparison of EddyPro and TK3, Atmos. Meas. Tech., 7, 2273–2281, https://doi.org/10.5194/amt-7-2273-2014, 2014.

Grosse, G., Romanovsky, V., Jorgenson, T., Anthony, K. W., Brown, J., and Overduin, P. P.: Vulnerability and feedbacks of permafrost to climate change, Eos, Transactions American Geophysical Union, 92, 73–74, 2011.

Harazono, Y., Mano, M., Miyata, A., Zulueta, R. C., and Oechel, W. C.: Inter-annual carbon dioxide uptake of a wet sedge tundra ecosystem in the Arctic, Tellus B, 55, 215–231, 2003.

Harris, C., Arenson, L. U., Christiansen, H. H., Etzelmüller, B., Frauenfelder, R., Gruber, S., Haeberli, W., Hauck, C., Hölzle, M., Humlum, O., Isaksen, K., Kääb, A., Kern-Lütschg, M. A., Lehning, M., Matsuoka, N., Murton, J. B., Nötzli, J., Phillips, M., Ross, N., Seppälä, M., Springman, S. M., and Vonder Mühll, D.: Permafrost and climate in Europe: Monitoring and modelling thermal, geomorphological and geotechnical responses, Earth-Sci. Rev., 92, 117–171, 2009.

Inagaki, A., Letzel, M. O., Raasch, S., and Kanda, M.: Impact of surface heterogeneity on energy imbalance: a study using LES, J. Meteor. Soc. Japn. Ser. II, 84, 187–198, 2006.

Johansson, M., Callaghan, T. V., Bosiö, J., Åkerman, H. J., Jackowicz-Korczynski, M., and Christensen, T. R.: Rapid responses of permafrost and vegetation to experimentally increased snow cover in sub-arctic Sweden, Environ. Res. Lett., 8, 035025, https://doi.org/10.1088/1748-9326/8/3/035025, 2013.

Jorgenson, M. T., Shur, Y. L., and Pullman, E. R.: Abrupt increase in permafrost degradation in Arctic Alaska, Geophys. Res. Lett., 33, L02503, https://doi.org/10.1029/2005GL024960, 2006.

Jorgenson, M. T., Kanevskiy, M., Shur, Y., Moskalenko, N., Brown, D. R. N., Wickland, K., Striegl, R., and Koch, J.: Role of ground ice dynamics and ecological feedbacks in recent ice wedge

degradation and stabilization, J. Geophys. Res.-Earth Surf., 120, 2280–2297, 2015.

Kljun, N., Calanca, P., Rotach, M. W., and Schmid, H. P.: A simple two-dimensional parameterisation for Flux Footprint Prediction (FFP), Geosci. Model Dev., 8, 3695–3713, https://doi.org/10.5194/gmd-8-3695-2015, 2015.

Kutzbach, L., Wille, C., and Pfeiffer, E.-M.: The exchange of carbon dioxide between wet arctic tundra and the atmosphere at the Lena River Delta, Northern Siberia, Biogeosciences, 4, 869–890, https://doi.org/10.5194/bg-4-869-2007, 2007.

Lara, M. J., McGuire, A. D., Euskirchen, E. S., Tweedie, C. E., Hinkel, K. M., Skurikhin, A. N., Romanovsky, V. E., Grosse, G., Bolton, W. R., and Genet, H.: Polygonal tundra geomorphological change in response to warming alters future CO_2 and CH_4 flux on the Barrow Peninsula, Glob. Change Biol., 21, 1634–1651, 2015.

Lee, X., Massman, W., and Law, B.: Handbook of micrometeorology: a guide for surface flux measurement and analysis, Springer Science & Business Media, Vol. 29, 2006.

Leffingwell, E. d. K.: Ground-ice wedges: The dominant form of ground-ice on the north coast of Alaska, J. Geol., 23, 635–654, 1915.

Liljedahl, A. K., Boike, J., Daanen, R. P., Fedorov, A. N., Frost, G. V., Grosse, G., Hinzman, L. D., Iijma, Y., Jorgenson, J. C., and Matveyeva, N.: Pan-Arctic ice-wedge degradation in warming permafrost and its influence on tundra hydrology, Nat. Geosci., 312–318, 2016.

Lucieer, A., Jong, S. M. D., and Turner, D.: Mapping landslide displacements using Structure from Motion (SfM) and image correlation of multi-temporal UAV photography, Prog. Phys. Geogr., 38, 97–116, 2014.

Lüers, J., Westermann, S., Piel, K., and Boike, J.: Annual CO_2 budget and seasonal CO_2 exchange signals at a high Arctic permafrost site on Spitsbergen, Svalbard archipelago, Biogeosciences, 11, 6307–6322, https://doi.org/10.5194/bg-11-6307-2014, 2014.

Lund, M., Falk, J. M., Friborg, T., Mbufong, H. N., Sigsgaard, C., Soegaard, H., and Tamstorf, M. P.: Trends in CO_2 exchange in a high Arctic tundra heath, 2000–2010, J. Geophys. Res.-Biogeo., 117, G02001, https://doi.org/10.1029/2011JG001901, 2012.

Mackay, J. R.: Ice-wedge cracks, Garry Island, Northwest Territories, Can. J. Earth Sci., 11, 1366–1383, 1974.

Mahrt, L., Sun, J., Vickers, D., MacPherson, J. I., Pederson, J. R., and Desjardins,, R. L.: Observations of fluxes and inland breezes over a heterogeneous surface, J. Atmos. Sci., 51, 2484–2499, 1994.

Mbufong, H. N., Lund, M., Aurela, M., Christensen, T. R., Eugster, W., Friborg, T., Hansen, B. U., Humphreys, E. R., Jackowicz-Korczynski, M., Kutzbach, L., Lafleur, P. M., Oechel, W. C., Parmentier, F. J. W., Rasse, D. P., Rocha, A. V., Sachs, T., van der Molen, M. K., and Tamstorf, M. P.: Assessing the spatial variability in peak season CO_2 exchange characteristics across the Arctic tundra using a light response curve parameterization, Biogeosciences, 11, 4897–4912, https://doi.org/10.5194/bg-11-4897-2014, 2014.

McGuire, A. D., Christensen, T. R., Hayes, D., Heroult, A., Euskirchen, E., Kimball, J. S., Koven, C., Lafleur, P., Miller, P. A., Oechel, W., Peylin, P., Williams, M., and Yi, Y.: An assessment of the carbon balance of Arctic tundra: comparisons among observations, process models, and atmospheric inversions, Biogeosciences, 9, 3185–3204, https://doi.org/10.5194/bg-9-3185-2012, 2012.

Minke, M., Donner, N., Karpov, N. S., de Klerk, P., and Joosten, H.: Distribution, diversity, development and dynamics of polygon mires: examples from Northeast Yakutia (Siberia), Peatlands International, 1, 36–40, 2007.

Moncrieff, J., Clement, R., Finnigan, J., and Meyers, T.: Averaging, detrending, and filtering of eddy covariance time series, in: Handbook of micrometeorology, Springer, 7–31, 2004.

Moncrieff, J. B., Massheder, J. M., De Bruin, H., Elbers, J., Friborg, T., Heusinkveld, B., Kabat, P., Scott, S., Soegaard, H., and Verhoef, A.: A system to measure surface fluxes of momentum, sensible heat, water vapour and carbon dioxide, J. Hydrol., 188, 589–611, 1997.

Natali, S. M., Schuur, E. A. G., Trucco, C., Hicks Pries, C. E., Crummer, K. G., and Baron Lopez, A. F.: Effects of experimental warming of air, soil and permafrost on carbon balance in Alaskan tundra, Glob. Change Biol., 17, 1394–1407, 2011.

Necsoiu, M., Dinwiddie, C. L., Walter, G. R., Larsen, A., and Stothoff, S. A.: Multi-temporal image analysis of historical aerial photographs and recent satellite imagery reveals evolution of water body surface area and polygonal terrain morphology in Kobuk Valley National Park, Alaska, Environ. Res. Lett., 8, 025007, https://doi.org/10.1088/1748-9326/8/2/025007, 2013.

Nordli, Ø., Przybylak, R., Ogilvie, A. E. J., and Isaksen, K.: Long-term temperature trends and variability on Spitsbergen: the extended Svalbard Airport temperature series, 1898–2012, Polar Res., 33, 21349, https://doi.org/10.3402/polar.v33.21349, 2014.

Oechel, W. C.: Seasonal patterns of temperature response of CO_2 flux and acclimation in Arctic mosses, Photosynthetica, 10, 447–456, 1976.

Oechel, W. C., Laskowski, C. A., Burba, G., Gioli, B., and Kalhori, A. A. M.: Annual patterns and budget of CO_2 flux in an Arctic tussock tundra ecosystem, J. Geophys. Res.-Biogeo., 119, 323–339, 2014.

Oliva, M., Vieira, G., Pina, P., Pereira, P., Neves, M., and Freitas, M. C.: Sedimentological characteristics of ice-wedge polygon terrain in Adventdalen (Svalbard) – environmental and climatic implications for the late Holocene, Solid Earth, 5, 901–914, https://doi.org/10.5194/se-5-901-2014, 2014.

Osterkamp, T. E., Jorgenson, M. T., Schuur, E. A. G., Shur, Y. L., Kanevskiy, M. Z., Vogel, J. G., and Tumskoy, V. E.: Physical and ecological changes associated with warming permafrost and thermokarst in interior Alaska, Permafrost Periglac., 20, 235–256, 2009.

Pirk, N., Tamstorf, M. P., Lund, M., Mastepanov, M., Pedersen, S. H., Mylius, M. R., Parmentier, F.-J. W., Christiansen, H. H., and Christensen, T. R.: Snowpack fluxes of methane and carbon dioxide from high Arctic tundra, J. Geophys. Res.-Biogeo., 121, 1–15, https://doi.org/10.1002/2016JG003486, 2016a.

Pirk, N., Mastepanov, M., Parmentier, F.-J. W., Lund, M., Crill, P., and Christensen, T. R.: Calculations of automatic chamber flux measurements of methane and carbon dioxide using short time series of concentrations, Biogeosciences, 13, 903–912, https://doi.org/10.5194/bg-13-903-2016, 2016.

Rastetter, E. B.: Validating models of ecosystem response to global change, BioScience, 46, 190–198, 1996.

Reichstein, M., Falge, E., Baldocchi, D., Papale, D., Aubinet, M., Berbigier, P., Bernhofer, C., Buchmann, N., Gilmanov, T., Granier, A., Grünwald, T., Havránková, K., Ilvesniemi, H., Janous, D., Knohl, A., Laurila, T., Lohila, A., Loustau, D., Matteucci, G., Meyers, T., Miglietta, F., Ourcival, J.-M., Pumpanen, J., Rambal, S., Rotenberg, E., Sanz, M., Tenhunen, J., Seufert, G., Vaccari, F., Vesala, T., Yakir, D., and Valentini, R.: On the separation of net ecosystem exchange into assimilation and ecosystem respiration: review and improved algorithm, Glob. Change Biol., 11, 1424–1439, 2005.

Romanovskii, N. N.: Distribution of recently active ice and soil wedges in the USSR, Field and Theory, 154–165, 1985.

Romanovsky, V. E., Smith, S. L., and Christiansen, H. H.: Permafrost thermal state in the polar northern hemisphere during the international polar year 2007–2009: a synthesis, Permafrost Periglac., 21, 106–116, 2010.

Sahlée, E., Smedman, A.-S., Rutgersson, A., and Högström, U.: Spectra of CO_2 and water vapour in the marine atmospheric surface layer, Bound.-Lay. Meteorol., 126, 279–295, 2008.

Schuur, E. A. G., McGuire, A. D., Schädel, C., Grosse, G., Harden, J. W., Hayes, D. J., Hugelius, G., Koven, C. D., Kuhry, P., Lawrence, D. M., and Natali, S. M.: Climate change and the permafrost carbon feedback, Nature, 520, 171–179, 2015.

Seok, B., Helmig, D., Williams, M. W., Liptzin, D., Chowanski, K., and Hueber, J.: An automated system for continuous measurements of trace gas fluxes through snow: an evaluation of the gas diffusion method at a subalpine forest site, Niwot Ridge, Colorado, Biogeochemistry, 95, 95–113, 2009.

Sievers, J., Sørensen, L. L., Papakyriakou, T., Else, B., Sejr, M. K., Haubjerg Søgaard, D., Barber, D., and Rysgaard, S.: Winter observations of CO_2 exchange between sea ice and the atmosphere in a coastal fjord environment, The Cryosphere, 9, 1701–1713, https://doi.org/10.5194/tc-9-1701-2015, 2015a.

Sievers, J., Papakyriakou, T., Larsen, S. E., Jammet, M. M., Rysgaard, S., Sejr, M. K., and Sørensen, L. L.: Estimating surface fluxes using eddy covariance and numerical ogive optimization, Atmos. Chem. Phys., 15, 2081–2103, https://doi.org/10.5194/acp-15-2081-2015, 2015.

Smagin, A. V. and Shnyrev, N. A.: Methane fluxes during the cold season: distribution and mass transfer in the snow cover of bogs, Eurasian Soil Sci., 48, 823–830, 2015.

Snavely, N., Seitz, S. M., and Szeliski, R.: Skeletal graphs for efficient structure from motion, in: CVPR, Vol. 1, p. 2, 2008.

Soegaard, H. and Nordstroem, C.: Carbon dioxide exchange in a high-arctic fen estimated by eddy covariance measurements and modelling, Glob. Change Biol., 5, 547–562, 1999.

Takagi, K., Nomura, M., Ashiya, D., Takahashi, H., Sasa, K., Fujinuma, Y., Shibata, H., Akibayashi, Y., and Koike, T.: Dynamic carbon dioxide exchange through snowpack by wind-driven mass transfer in a conifer-broadleaf mixed forest in northernmost Japan, Global Biogeochem. Cy., 19, GB2012, https://doi.org/10.1029/2004GB002272, 2005.

Tieszen, L. L., Miller, P. C., and Oechel, W. C.: Photosynthesis, in An arctic ecosystem: the coastal tundra at Barrow, Alaska, Dowden, Hutchinson & Ross, Inc, 1980.

Ullman, S.: The interpretation of structure from motion, P. Roy. Soc. London B, 203, 405–426, 1979.

Vaughn, L. J. S., Conrad, M. E., Bill, M., and Torn, M. S.: Isotopic insights into methane production, oxidation, and emissions in Arctic polygon tundra, Glob. Change Biol., 22, 3487–3502, https://doi.org/10.1111/gcb.13281, 2016.

Vickers, D. and Mahrt, L.: Quality control and flux sampling problems for tower and aircraft data, J. Atmos. Ocean. Technol., 14, 512–526, 1997.

Wegener, C. and Odasz-Albrigtsen, A. M.: Do Svalbard reindeer regulate standing crop in the absence of predators?, Oecologia, 116, 202–206, 1998.

Westoby, M. J., Brasington, J., Glasser, N. F., Hambrey, M. J., and Reynolds, J. M.: "Structure-from-Motion" photogrammetry: A low-cost, effective tool for geoscience applications, Geomorphology, 179, 300–314, 2012.